Available online at www.sciencedirect.com

SciVerse ScienceDirect

Journal of the European Ceramic Society 32 (2012) 1837–1845

www.elsevier.com/locate/jeurceramsoc

Aerothermal behaviour of a SiC fibre-reinforced ZrB_2 sharp component in supersonic regime

Diletta Sciti [a], Raffaele Savino [b], Laura Silvestroni [a,*]

[a] *CNR-ISTEC, Institute of Science and Technology for Ceramics, Via Granarolo 64, I-48018 Faenza, Italy*
[b] *Department of Aerospace Engineering, University of Naples "Federico II" – P.le Tecchio 80, 80125, Naples, Italy*

Received 12 September 2011; received in revised form 12 December 2011; accepted 16 January 2012
Available online 16 February 2012

Abstract

The aerothermal behaviour of a SiC fibre-reinforced ZrB_2 composite machined in a sharp-shaped component with a tip curvature radius of 0.1 mm was investigated using an arc-jet facility. The specimen underwent 4 thermal cycles and the emissivity was evaluated in the temperature range 1000–1700 °C. The temperature profile along the specimen was calculated through computational fluid dynamic (CFD) modelling. The microstructural evolution was compared to a typical ZrB_2 composite containing the same amount of SiC in particulate form, which underwent similar aerodynamic conditions.

Keywords: ZrB_2; SiC fibre; Arc-jet; Atmospheric re-entry; Oxidation

1. Introduction

Ultra-high temperature ceramics (UHTCs) are currently considered promising materials for aerospace applications as hypersonic and propulsion parts of new generation aircrafts.[1–3] In fact, the oxidation and ablation behaviour of UHTC composites based on ZrB_2 and SiC proved to be better than the C/C composites actually used in the aerospace industry, owing to the low oxygen diffusion rate of the formed glass and the supporting role of the solid ZrO_2 skeleton.[4] Actually, the oxidation behaviour of ZrB_2–SiC particles composites has been extensively studied in static and flowing air, long and short term and at different conditions of oxygen partial pressure.[5–10] However, to assess the aerothermal behaviour of UHTCs, the most representative experiment that simulates the extreme conditions experienced by materials during re-entry in atmosphere is arc-jet testing. The material response to large heat fluxes is evaluated not only through the analysis of oxidation products, but also through the determination of its emissivity. High values of emissivity are desired for space applications, in order to reduce temperature gradients and thermal stresses in the structure, thus enabling the vehicle to operate under relatively high enthalpy flow conditions. Due to the limited number of accessible arc-jet facilities and the high costs of the experiments, available data on the behaviour of UHTC under simulated re-entry conditions are very scarce and furthermore it is not possible to make comparisons between different tests owing to the discrepancy between the precise material composition, the operating conditions and response of the material.

As for ablation testing or oxidation at very high temperature of ZrB_2–SiC ceramics, an increasing number of studies have been performed on composites with variable SiC amount,[11] in the temperature range from 1700 °C up to 2300 °C, on flat, curved or sharp models,[12,13] under subsonic to supersonic conditions,[14] using oxyacetylene torch or plasma wind tunnel in air.[15–17] All these studies agreed that after exposure to high heat fluxes at temperature up to 1800 °C, the formation of a stable multiphase oxide scales and the high thermal conductivity were responsible of the success of the material in such conditions. However, for temperatures in the order of 2300 °C, strong ablation occurred and the material was unable to offer a valuable resistance to the applied aerothermal load.

The arc-jet studies extended to other UHTCs as potential components in sharp leading edge applications, either in

* Corresponding author. Tel.: +39 0546 699 723; fax: +39 0546 46381.
E-mail address: laura.silvestroni@istec.cnr.it (L. Silvestroni).

0955-2219/$ – see front matter © 2012 Elsevier Ltd. All rights reserved.
doi:10.1016/j.jeurceramsoc.2012.01.019

the ZrB_2–SiC system with addition of other transition metals borides and carbides,[18] or to different matrices, such as HfB_2, combined with SiC, $TaSi_2$ or $MoSi_2$.[1,19,20]

In this work, for the first time, we report the behaviour of a new ZrB_2-based composite containing short SiC fibre (SiCf) upon arc-jet testing. This kind of composite has been specifically designed to improve the fracture toughness of brittle ZrB_2 ceramics containing SiC particles (SiCp), but its behaviour under extreme conditions is not known. Furthermore, different from previous published works, the material was machined in a very sharp profile. It is well known that nosecones and wing leading edges with sharp profiles, with curvature radius in the order of few millimetres, enable the vehicle to enhance the performances and the manoeuvrability by reducing the friction drag, and also to improve the crew safety, owing to increased cross range capability. However, smaller tip radius implies higher temperature achieved during re-entry and such extremely high temperature cannot be withstood by conventional materials used for thermal protection systems.

Fluid dynamic numerical simulations were carried out in order to rebuild the experimental conditions and to evaluate the temperature gradient along the sharp profile with respect to the material response.

The ultimate purpose of the paper is to assess whether the replacement of SiC particles by short fibres significantly affects the oxidation behaviour. Hence, comparison is made with a ZrB_2–SiCp model processed under the similar conditions.[13]

2. Experimental

2.1. Material processing and characterisation

The material under investigation had the following composition: ZrB_2 + 5 vol% Si_3N_4 + 20 vol% SiC chopped fibres. Commercial powder were used to produce the composite: ZrB_2 Grade B (H.C. Starck, Goslar, Germany), specific surface area 1.0 m^2/g, maximum impurity content (wt%): 0.25C, 2O, 0.25N, 0.1Fe, 0.2Hf, particle size range 0.1–8 μm; α-Si_3N_4 Baysinid (Bayer, Leverkusen, Germany), specific surface area 12.2 m^2/g, impurity maximum content (wt%): 1.5O; SiC Hi-Nicalon chopped fibres with composition Si:C:O = 62:37:0.5 wt%, diameter 14 μm and 1 mm length. The powder mixture was gently ball milled for 24 h in absolute ethanol using silicon carbide media and the slurry was subsequently dried in a rotary evaporator. The powder mixture was debonded at 600 °C/h up to 500 °C for 30 min prior to sintering. Hot-pressing was conducted in low vacuum (~100 Pa) using an induction-heated graphite die with uniaxial pressure of 30 MPa during the heating at 900 °C/h and increased up to 40 MPa at 1700 °C. Pressure was removed after 10 min at this temperature and free cooling followed. Further details on the materials preparation, densification, microstructure and mechanical properties have been reported in a previous work.[21] From the dense billet a sharp shaped specimen was machined (Fig. 1a), with tip radius of 0.1 mm and total length from the base of 15 mm.

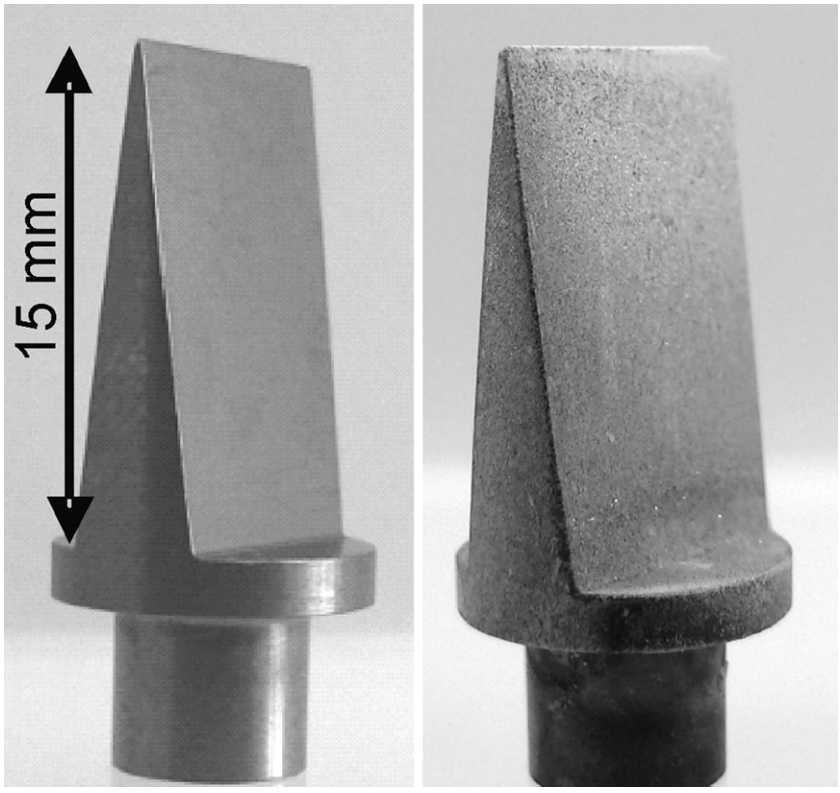

Fig. 1. Sample before (left) and after (right) the torch tests.

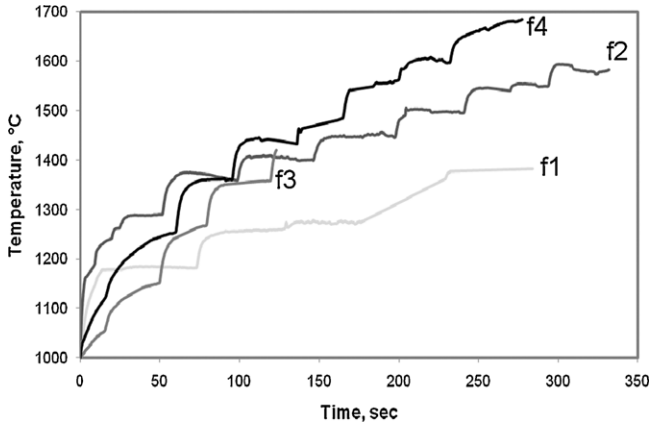

Fig. 2. Temperature jumps recorded by the thermograph during the 4 runs as a function of time. Each temperature step represents an enthalpy increase in input.

2.2. Plasma torch tests

The experiments have been carried out in the Small Planetary Simulator facility (SPES) available at the Dept. of Aerospace Engineering (DIAS) of the University of Naples.

SPES is an arc-jet facility equipped with a 80 kW plasma torch that operates with inert gases at mass flow rates up to 5 g/s. In order to simulate the air composition, oxygen can be mixed to primary nitrogen jet using a swirling jet in the mixing chamber after the torch. A detailed description of the facility and of its typical performances can be found in Ref. 13, where similar tests on UHTC spherical specimens are described. For the present experiments a supersonic nozzle with nominal Mach number $M = 3$ was utilised. The gas mass flow rate was fixed at 1 g/s, the specimen was located at a distance of 1 cm from the exit nozzle and the heating level adjusted by incrementally increasing the arc power (from 15 kW to 36 kW). As described in 13, when arc voltage and current increase, the total enthalpy of the flow gradually increases too and also the Pitot pressure changes with the arc power. Estimated average specific total enthalpy (H0) and maximum stagnation point pressure (P_{max}) ranged between 8 and 16.4 MJ/kg and 6 and 12 kPa, respectively.

The ZrB_2-based model was exposed to hot streams at different conditions as plotted in Fig. 2 and Table 1. The total time of exposure was around 17 min in four different oxidation cycles. During the experiments, infrared and optical windows in the test chamber allowed visual inspection and diagnostic analyses. An automatic control system monitored the main parameters of the apparatus (voltage and current of the arc heater, water cooling temperature, mass flow rate). In particular, the specific total enthalpy was evaluated through an energy balance between the energy supplied to the gas by the arc heater and the energy transferred to the cooling system. The output data, processed via dedicated software, allowed the evaluation of the surface temperature profile versus exposure time of the model. Due to the extremely high thermal loading upon the ceramic models, surface chemical reactions like oxidation can be responsible for changes in the material emissivity. To overcome this problem, the measurements were carried out with a radiation ratio pyrometer (Infratherm ISQ5, Impac Electronic Gmbh, Germany), focussed on a 3-mm diameter spot on the tip, which operates both in two colours and in the single colour function. In the two-colour mode the instrument makes use of the ratio between two spectral radiances, measured at different wavelengths (0.9–1.05 μm), to evaluate the real temperature. Once the temperature was measured with the ratio pyrometer, its value was input to evaluate the spectral emissivity using the single colour function. In combination with the pyrometer, an infrared thermo-camera (Thermacam SC 3000, FLIR Systems, USA) was used to measure the surface temperature distributions, using the spectral emissivity in the long wave range of the thermograph ($\lambda = 9$ μm), obtained on the basis of the temperature measured by the two-colour pyrometer.

Table 1
Summary of maximum enthalpy, total times of each run, maximum temperature achieved, emissivity measured by the pyrometer and total time of exposure to the hot stream for ZrB_2–SiCf and ZrB_2–SiCp composites.

Test	$H0_{max}$ (MJ/kg)	Time (s)	T_{max} (°C)	ε	Total time
f1	13.8	285	1380	0.88	
f2	17.0	330	1590	0.86	
f3	12.3	120	1395	0.65	16′ 45″
f4	17.0	270	1680	0.54	
p1	10	240	1780	0.63	4′

3. Results and discussion

3.1. Microstructural features of the as-sintered sample

The SiC fibre reinforced UHTC sample was fully dense with mean grain size around 2 μm. The secondary phases observed in the sintered microstructure were mainly concentrated at triple points and were identified by SEM–EDS as ZrO_2, BN, Zr–Si phases and a borosilicatic glass containing Zr–Si–B–N–O. The dispersion of the fibres into the matrix was homogeneous, since no agglomeration was observed. Porosity was nearly absent and no microcracking was noticed. Hi-Nicalon fibres are constituted by nanocrystalline grains of beta SiC, an amorphous Si–C–O phase and residual C.[22] After sintering of the composite, the fibres showed a multilayered core–shell morphology: the inner part was constituted by stoichiometric SiC and the surrounding shell was Si–C–O with embedded ZrC crystals, see Fig. 3.

3.2. Temperature profile and emissivity

The pyrometer was focused into a 3-mm wide spot looking at the large model surface from the side and it provided the average temperature of this area. Due to the sharpness of the specimen, it is reasonable that the temperature is maximum at the leading edge, where the maximum heat flux is experienced, and then rapidly decreases moving towards the backward part. Since the actual temperature experienced on the tip was not measured, computational fluid dynamic (CFD) simulations were carried out using the method presented in 17, taking into account thermal and chemical non-equilibrium, surface catalysis properties, the

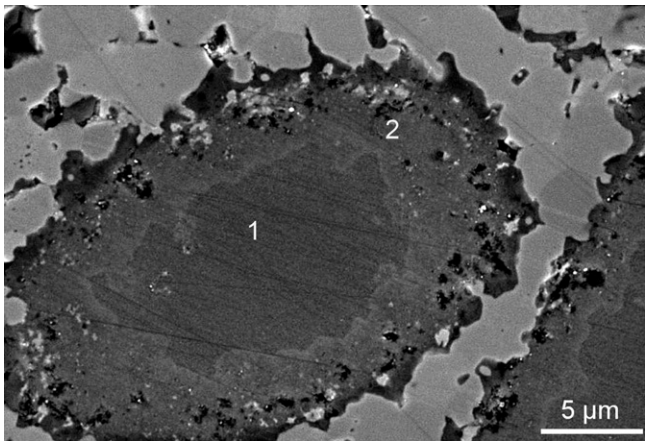

Fig. 3. Fibre–matrix interface morphology of the as sintered composite: 1: SiC core, 2: SiCO shell with ZrC particles embedded in.

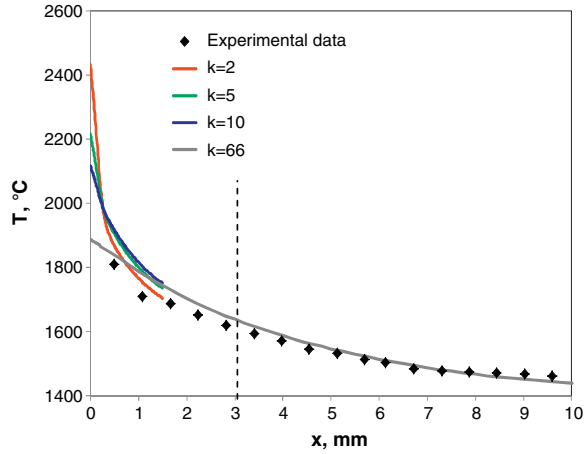

Fig. 4. Temperature trend as a function of the distance from the tip and the thermal conductivity. Experimental data recorded by thermograph and CFD simulations with different k values in input. From 1.5 mm downwards k is considered the same as the original ZrB_2–SiC ceramic. The vertical dotted line marks the 3-mm diameter measured by the pyrometer.

change of the surface temperature during the test, the radiation emitted from the surface at relatively high temperature and the presence of a layered multicomponent oxide scale.

In particular, the CFD model was based on the solution of the Navier–Stokes equations for a mixture of reacting species in chemical and vibrational non-equilibrium. The computed surface heat flux distributions have been used to evaluate the thermal distribution in the solid UHTC, solving the unsteady energy equation in the solid, with the surface heat flux updated at each iteration to account for the energy re-emitted radiatively and for the changes in convective heat flux due to changes in surface temperature. Details on the calculation procedure are presented in Ref. 23. It has been already reported that the formation of oxidation products, such as zirconia, causes a change in the surface emissivity and thermal conductivity that in turn affects the ability to re-emit heat. After the 3rd and 4th run the emissivity decreased to around 0.65 and 0.55, respectively, and these values, which are typical of zirconia at high temperature,[24] are in agreement with microstructural observations of the tip oxide scale (see Section 3.3).

For the present analysis, different thermal conductivities have been considered as input of the heat conduction code: a value of 66 W/(m K) for the unoxidised part of the UHTC specimen, and different values for the oxidised portion (tip) of the model. A value of 2 W/(m K) is the most reasonable considering that the majority of the oxidised surface is composed by zirconia. Using this input value for thermal conductivity and 0.6 for total emissivity, radiative equilibrium temperatures in excess of 2400 °C at the maximum H0 were calculated to occur on the model tip (Fig. 4). Furthermore, these data, in conjunction with the thermograph profile, enabled the reconstruction of the temperature gradient as a function of the model profile, where the tip is mainly constituted by zirconia, possessing low thermal conductivity down to the first 1.5 mm, and then the conductivity is considered the same as that of typical of ZrB_2–SiC composites (Fig. 4). It is interesting to note that the temperature dropped very steeply to 1800 °C at a distance of about 1 mm from the tip and to 1600 °C at a distance of 3 mm.

3.3. Microstructural modifications induced by oxidation

Fig. 1 shows the appearance of the model before and after the test. No appreciable shape modification occurred: the profile is maintained and the colour of the tested sample looks whitish in the tip and gradually becomes darker down to the base. A white appearance, both by eye and by SEM, is an indication of ZrO_2 phase, whilst darker regions imply the presence of silica-based glass.

External surface: The first 450 μm of the external surface of the model are displayed in the SEM image of Fig. 5a. The morphology appeared very diverse depending on the distance from the tip. The most damaged area was the summit of the sample (Fig. 5b), where only ZrO_2 phase was observed together with cracks, porosities and C traces. Moving few tens of microns from the tip down to about 300 μm (Fig. 6a), an interesting feature was the presence of large amounts of carbon residues filling the cavities left by SiC fibres. The disappearance of the SiC phase confirms that the real peak temperature achieved in this part was higher than 1700 °C as measured by the pyrometer.[9]

At a distance of about 300 μm from the tip, the fibre cast was recognisable, but was constituted by tiny and curly ZrO_2 agglomerates filled by silica-based glass (Fig. 6b), moving further downwards the aspect was inverted, i.e. pools of silica were noticed mainly where fibres were originally located, containing small ZrO_2 precipitates (Fig. 6c). Glass bubbles and pores suggestive of bursting events indicate silica melting and vaporisation (Fig. 6d); in these surface regions, the formation of silica was generally discontinuous (Fig. 6e). At 6 mm the surface morphology gradually changed, showing unoxidised or partially oxidised SiC fibres and ZrO_2 particles (Fig. 6f).

Cross section: Cross-sectioning the model resulted in damage by the polishing procedure, indicating a brittle nature of the oxide layer (Fig. 7a). However the three typical regions observed for ZrB_2–SiC composites were recognisable: an outermost cracked zirconia layer with carbon agglomerates,

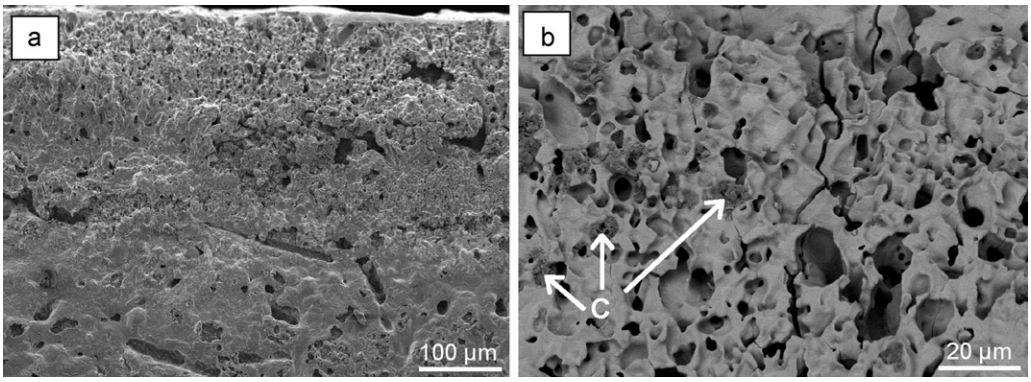

Fig. 5. External morphology of the ZrB_2–SiCf composite after exposure to 4 runs, (a) first 450 μm and (b) magnification of the first 100 μm where C residuals are indicated by arrows.

a ZrO_2 interlayer containing melted silica at the place where fibres were originally located, having a thickness of approximately 120 μm (Fig. 7b) and a SiC-depleted ZrB_2 region, about 400 μm thick. Surprisingly, rounded grains of zirconia were observed instead of typical columnar structures. The thickness of the external ZrO_2 layer varied from 120 μm on the summit to 40–50 μm on the sides.

Evidences of spallation were observed between the first two ZrO_2-based layers and the SiC-depleted ZrB_2 layer, owing to ZrO_2 tetragonal to monoclinic phase transformation.

Approximately at 600 μm from the tip, an early stage oxidation of the fibres could be observed (Fig. 7c): the core was SiC which was oxygen enriched moving outward, and, around the fibre, a continuous graphite layer was observed, indicating a double process for SiC oxidation including formation of SiO_2 and C. This progressive fibre corrosion and thinning was confirmed by observation of SiC-based elongated structure right below the SiC-depleted region.

Distinctly from conventional ZrB_2–SiCp composites, upon oxidation, the presence of carbon residuals was very clear, both in the external surface (Fig. 6a) and in the cross section (Fig. 7b). It is apparent that SiC fibres oxidised through different mechanisms as compared to what generally occurs for SiC particles.

3.4. Oxidation mechanisms of SiC fibres in the ZrO_2 scale

One of the most interesting features of this study is the oxidation mode of SiC fibres in ZrB_2 matrix, especially concerning the formation of carbon residuals. Hi-Nicalon SiC fibres have a microstructure constituted by β-SiC nanocrystallites, free carbon and an amorphous silicon oxycarbide phase. Hence, their mode of oxidation can significantly differ from that of SiC particles. As a matter of fact, high temperature oxidation of Hi-Nicalon fibres has been studied by several authors up to 1500 °C.[25,26] Thermodynamic investigations by Vahlas et al. have shown that upon certain oxidation conditions a free carbon interphase is produced between the external silica layer and

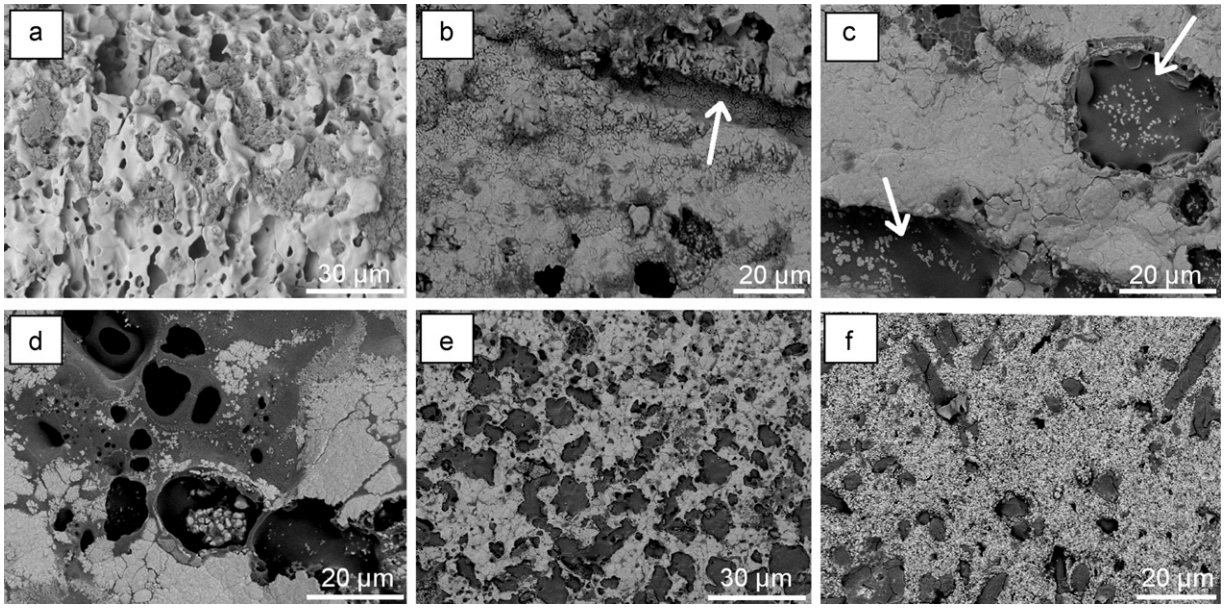

Fig. 6. Appearance of the external surface of the wedge. Distance from the tip: (a) 100 μm, (b) 300 μm, (c) 400 μm, (d) 1 mm, (e) 3 mm, (f) 6 mm. Arrows in (b) and (c) indicate where the fibres were originally located.

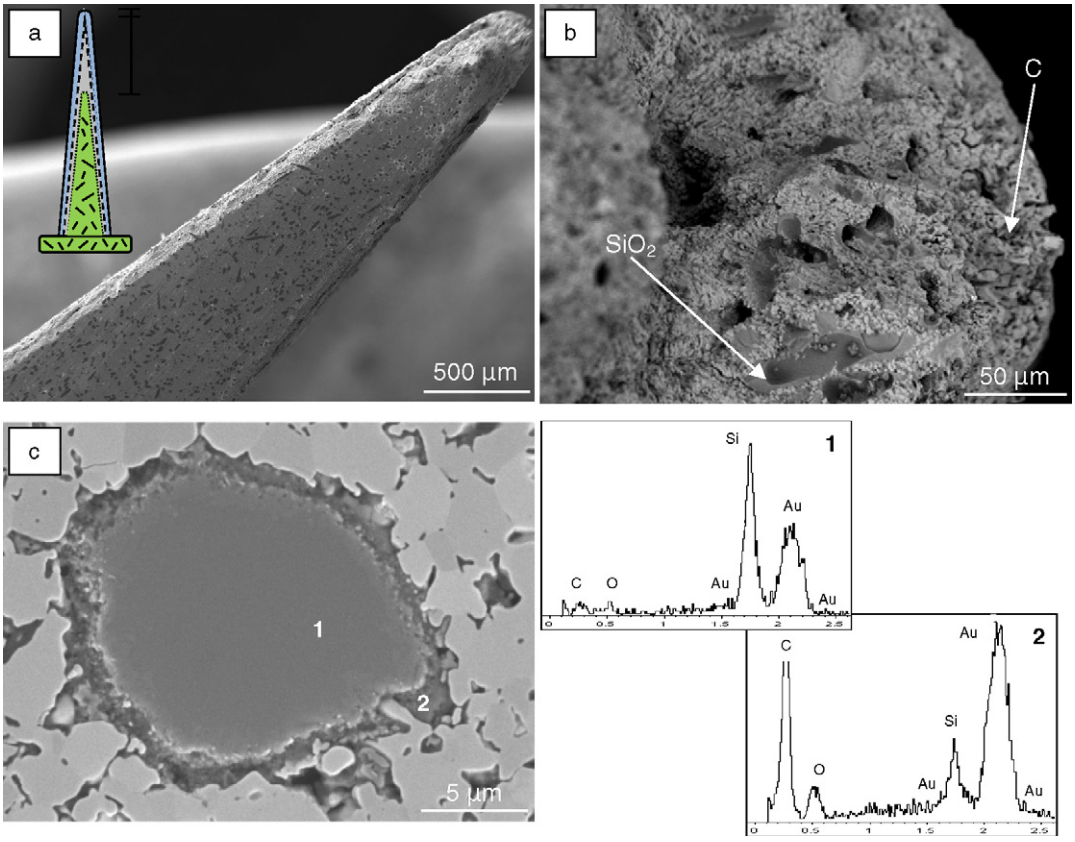

Fig. 7. Cross section of the ZrB_2–SiCf composite after exposure to 4 runs. (a) Overview and sketch of the layers, from inside: original UHTC, SiC-depleted ZrB_2, external ZrO_2 containing silica and C traces. (b) magnification of the tip region indicating C traces and SiO_2 immersed in ZrO_2, (c) fibre morphology below the SiC depletion zone with the corresponding EDS spectra.

the unaffected SiC core and that at low atmospheric pressure an active oxidation process takes place. On the other hand, Shimoo et al.[26] observed that Hi-Nicalon fibres oxidation behaviour is affected by the presence of the unstable grain boundary phase based on $Si_xC_yO_z$ whose decomposition into gaseous SiO and CO can be suppressed only if a stable silica layer is formed on the fibre surface. By thermodynamic calculations, they found that during oxidation at 1500 °C, a stable silica film forms on the fibre surface only if the oxygen partial pressure is $>2.5 \times 10^2$ Pa. For values in the range 10^2–10^3 Pa an intermediate carbon layer and silica are produced, but at lower pressures an active oxidation prevails with serious mass loss and fibre pulverisation.

When considering the fibres dispersed into the boride matrix, one should keep in mind that the fibre during sintering develops a layered structure, as displayed in Fig. 3. Preferential migration of the $Si_xC_yO_z$ interphase from grain boundaries to the fibre surface generates the mentioned core–shell structure, with a SiC core and $Si_xC_yO_z$ phase shell containing ZrC small grains. Hence the dominant oxidation mechanism for the fibres first involves the external $Si_xC_yO_z$ phase.

At the most extreme conditions on the sample tip, complete decomposition of the external $Si_xC_yO_z$ layer and the SiC core occurs due to the instability of both phases at temperatures >2300 °C. This leaves only monoclinic zirconia as the outermost layer. Just a few micrometers away from the tip, decomposition of the fibres only left traces of carbon, as observed by SEM. In such extreme conditions, it is not possible to assess whether carbon residuals are those originally present in the fibre structure or are newly formed. From 300 µm to 3 mm, the temperature on the surface drops very fast from above 2000 °C to values around 1600–1700 °C (see temperature profile in Fig. 4) and the oxygen partial pressure is compatible with passive oxidation conditions, i.e. about or slightly lower than 10^2 Pa.[26] Hence oxidation of the $Si_xC_yO_z$ phase is expected to occur through two possible reactions:

$$Si_xC_yO_z + (x - 0.5z)O_2(g) = xSiO_2(s) + yC(s) \quad (1)$$

$$Si_xC_yO_z + (x + 0.5y - 0.5z)O_2(g) = xSiO_2(s) + yCO(g) \quad (2)$$

The observation of carbon residues indicates that reaction (1) is very likely to occur. Residual zirconia crystallites observed in the silica pools, Fig. 6c, could derive from oxidation of ZrC crystallites originally embedded in the layered structure of the fibre (see Fig. 3), given the same mean grain size around 400 nm. Although oxidation by reactions (1) and (2), leads to formation of silica, at these temperatures silica is not stable or it is removed by the hot stream such that no continuous coverage of the ZrO_2 layer is found. In the portion of material comprised between 3 and 6 mm, measured temperatures are lower than 1600 °C and the external oxide layer resembles that of materials oxidised in conventional furnace at temperature between 1200 and 1700 °C.[27]

In the *cross section*, under the outermost zirconia layer, only silica residuals are found of the original SiC fibres. In this case it is hypothesised the following mechanisms to occur:

- decomposition of the external $Si_xC_yO_z$ fibre layer into gaseous products (SiO, CO, CO_2);
- oxidation of the SiC core with formation of a SiO_2 and gaseous products, similarly to SiC particles.

In the depletion layer, due to very low oxygen partial pressure, an active oxidation of the fibres occurs, similar to what happens during oxidation of ZrB_2–SiCp composites. Again, active oxidation starts from the external $Si_xC_yO_z$ layer, eventually involving the inner SiC core. Possible reactions reported in the literature for the silicon oxycarbide phase[26] are revised as follows:

$$Si_xC_yO_z + (x - z)/2O_2(g) = xSiO(g) + yC(s) \quad (3)$$

$$Si_xC_yO_z + (x + y - z)/2O_2(g) = xSiO(g) + yCO(g) \quad (4)$$

$$Si_xC_yO_z + (x + 2y - z)/2O_2(g) = xSiO(g) + yCO_2(g) \quad (5)$$

At the border between the depletion layer and the unaffected core, an early stage of fibre oxidation can be observed showing the removal of the $Si_xC_yO_z$ phase and formation of the C interlayer. Progressively, the elimination of the $Si_xC_yO_z$ external shell also causes detachment from the matrix and further fibre consumption and thinning. From reactions (2), (4) and (5) it is apparent that $Si_xC_yO_z$ and SiC oxidation is accompanied by a large generation of CO/CO_2 species. If the escape of these gases is hindered by a compact ZrO_2–SiO_2 oxide, fibre sites are saturated in CO and the formation of graphite is further on favourable:

$$SiC + CO = 2C + SiO \quad (6)$$

This could be another reason explaining the presence of carbon agglomerates around the fibre just in the transition area between the SiC-depleted zone and the unreacted bulk. The formation of carbon film was already reported in a study on the thermal stability of Hi-Nicalon fibres at high temperatures in carbon monoxide[28] and more specifically during oxidation in ZrB_2–SiC composites.[9,12]

3.5. Aerothermal behaviour: comparison between SiCp and SiCf

It is now worth to make a brief comparison between the oxidation behaviour of the present composite and that of ZrB_2–SiCp model previously tested under similar aerothermal conditions.[13]

The previously tested ZrB_2–SiCp model was produced in ISTEC labs and contained the same amount of SiC phase in particles (20 vol%), the same type of sintering aid (Si_3N_4) and similar fractions of secondary glassy phases. Different from the present case, the geometry of ZrB_2–SiCp model was a blunt one.

Thermal conductivity of the two composites, as tested by the laser flash method, was very similar and varied from 75 to 46 W/(m K) at 25 °C and 1500 °C respectively, for ZrB_2–SiCp,[13] and 66 W/(m K) at room temperature to 50 W/(m K) at 1500 °C for ZrB_2–SiCf.

As for the arc-jet tests, the material containing particles was subjected to one single run with peak temperature around 1780 °C for a total time of about 4 min,[13] instead of four runs for a total time of about 17 min for the material containing fibres (Table 1). As a consequence, emissivity values were slightly higher for the ZrB_2–SiCp (0.62), owing to partial preservation of silica on the tip region.[13] For the model containing fibres, the high temperatures, the multiple tests and overall time of exposure caused the emissivity to decrease to 0.65 and 0.54 after 3° and 4° runs, respectively (Table 1). In spite of that, the SiC fibre reinforced material response is believed to be not substantially different from that of the SiC particle one.

Concerning the oxidation products, the external oxide of the ZrB_2–SiCp composite was basically constituted by porous columnar zirconia on the tip and, from 2 mm downwards, an almost continuous silica scale with distinct zirconia islands was detected.[13] In contrast, for the ZrB_2–SiCf a continuous silica layer was never observed, and the outermost layer was equiaxial zirconia with carbon residues. Whilst this novel aspect deserves further investigation, possible reasons for these diverse morphologies could be based on the different distribution of the SiC phase in the ZrB_2 matrix, which is in turn related to the different SiC morphology. The oxidation of ZrB_2–SiC composites is well known at the state of the art.[5,7–12,29] Below 1200 °C the oxidation rate of SiC is much lower than that of ZrB_2, but as the temperature approaches 1300 °C, SiC begins to markedly oxidise, resulting in the formation of a continuous surface layer above the ZrO_2 layer. ZrB_2 and SiC have a similar oxidation rates in the temperature range of 1300 °C to approximately 1600 °C and the oxide growth is dominated by the inward movement of the reaction interface. Active oxidation of SiC is observed in the temperature range of 1600–1700 °C, which causes a significant increase in the oxidation rate of SiC leading to its preferential oxidation.[9] The change in the relative oxidation rates of ZrB_2 and SiC alters the oxygen diffusion route, resulting in a different oxidation mechanism. In addition, the relative oxidation rate will change the inner structure of the oxide scale which strongly depends on SiC distribution. The preferential consumption of SiC particles due to active oxidation promotes the generation of pores in the oxidation reaction region. According to the work of Hu et al.[9] in the depletion region a porous layer will only develop when the amount of SiC is above the threshold for forming a 3D interconnected network. The percolation limit is in turn dependent on the SiC dimensions and dispersion. Fig. 8 shows the image analysis performed on the starting microstructure of the ZrB_2–SiCp and ZrB_2–SiCf composites. It can be observed that the minimum distance between the closest SiC particles is around 1.5 μm, whilst in the case of fibres the minimum distance is in the order of 25 μm. This aspect of course must have induced different oxidation mechanisms and/or different oxidation rates, which at the moment are not exactly known. For instance, that fact that particles were better interconnected suggests that they oxidised faster than the fibres, that behave more like isolated oxidation sites.

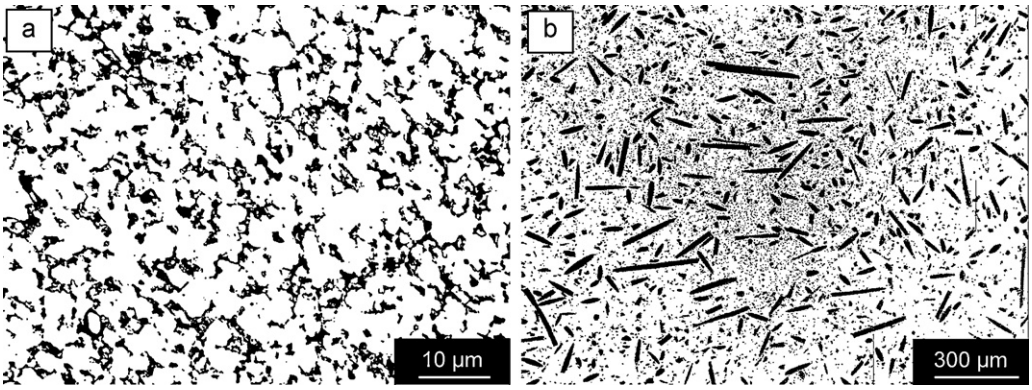

Fig. 8. Image analysis comparing the microstructure of ZrB_2-based ceramic containing 20 vol% SiC in form of (a) particulates and (b) fibres.

The effect of carbon residuals on the external oxide scale is another unexplored issue. The presence of significant amounts of carbon on the surface could have affected emissivity and thermal conductivity of the material, which in turn can change the maximum temperatures achieved on the tip. Just assuming slightly higher thermal conductivities, about 10 W/(m K), it can be observed in Fig. 4 that the maximum peak temperatures decrease of more than 300 °C. This aspect deserves further investigation, but suggests the fibre-reinforced material, besides having a twofold toughness, could a have better aerothermal behaviour than ZrB_2–SiCp composites.

4. Conclusions

The aerodynamic behaviour of a very sharp ZrB_2-based composite containing SiC short fibres was tested in a wind plasma tunnel in supersonic regime. A wedge with curvature radius of 0.1 mm was exposed to four runs in a temperature range 1400–1700 °C for a total time of about 17 min. The microstructural modifications induced by the hot stream were used as input values for computational fluid dynamics which furnished as output the temperature gradient along the wedge profile and pointed out a peak temperature on the tip in excess of 2300 °C. The wedge survived the test with minimal dimension or shape change.

The tip was externally constituted by zirconia and carbon residues which replaced the fibre sites. Moving downwards, silica-based glass appeared at around 350 μm and at 3 mm the surface was composed by discontinuous silica glass immersed into zirconia phase. The cross section displayed the typical layered morphology of ZrB_2–SiCp composites, with the only difference being the presence of carbon in the outermost zirconia scale.

The comparison with ZrB_2 ceramics containing the same amount of SiC, but in particulate form, exposed to similar aerodynamic conditions in the same arc-jet facility revealed that the material containing fibre did not perform worse than the one containing SiC particles. This comparison also suggested that the outer morphology of the oxide scale can be affected by the dimension and distribution of the SiC phase and formation or not of a SiC percolating network.

Acknowledgement

F. Monteverde is acknowledged for the fruitful discussions on thermal behaviour.

References

1. Gasch M, Ellerby D, Irby E, Beckman S, Gusman M, Johnson S. Processing, properties and arc jet oxidation of hafnium diboride/silicon carbide ultra-high temperature ceramics. *J Mater Sci* 2004;**39**:5925–37.
2. Wuchina E, Opeka M, Causey S, Buesking K, Spain J, Cull A, et al. Designing for ultrahigh-temperature applications: the mechanical and thermal properties of HfB_2, HfC_x, HfN_x and αHf(N). *J Mater Sci* 2004;**39**: 5939–49.
3. Gasch M, Ellerby D, Johnson S. Ultra high temperature ceramic composites. In: Bansal NP, editor. *Handbook of ceramic composites*. Boston: Academic Press; 2005. p. 197–224.
4. Tang SF, Deng JY, Wang SJ, Liu WC, Yang K. Ablation behaviors of ultra-high temperature ceramic composites. *Mater Sci Eng A* 2007;**465**:1–7.
5. Fahrenholtz WG. Thermodynamic analysis of ZrB_2–SiC oxidation: formation of a SiC-depleted region. *J Am Ceram Soc* 2007;**90**:143–8.
6. Monteverde F, Bellosi A. Oxidation of ZrB_2-based ceramics in dry air. *J Electrochem Soc* 2003;**150**:B552–9.
7. Li J, Lenosky TJ, Först CJ, Yip S. Thermochemical and mechanical stabilities of the oxide scale of ZrB_2-SiC and oxygen transport mechanisms. *J Am Ceram Soc* 2008;**91**:1475–80.
8. Karlsdottir SN, Halloran JW. Oxidation of ZrB_2–SiC: influence of SiC content on solid and liquid oxide phase formation. *J Am Ceram Soc* 2009;**92**:481–6.
9. Hu P, Guolin W, Wang Z. Oxidation mechanism and resistance of ZrB_2–SiC composites. *Corros Sci* 2009;**51**:2724–32.
10. Bongiorno A, Först CJ, Kalia RK, Li J, Marschall J, Nakano A, et al. A perspective on modeling materials in extreme environments: oxidation of ultrahigh-temperature ceramics. *Mater Res Soc Bull* 2006;**31**:410–8.
11. Chamberlain AL, Fahrenholtz WG, Hilmas G, Ellerby D. Oxidation of ZrB_2–SiC ceramics under atmospheric and reentry conditions. *Refract Appl Trans* 2005;**1**:1–8.
12. Monteverde F, Savino R, De Stefano Fumo M. Dynamic oxidation of ultra-high temperature ZrB_2–SiC under high enthalpy supersonic flows. *Corros Sci* 2011;**53**:922–9.
13. Savino R, De Stefano Fumo M, Paterna D, Di Maso A, Monteverde F. Arc-jet testing of ultra-high-temperature-ceramics. *Aerosp Sci Technol* 2010;**14**:178–87.
14. Zhang XH, Hu P, Han JC, Meng SH. Ablation behavior of ZrB_2–SiC ultra-high temperature ceramics under simulated atmospheric re-entry conditions. *Comp Sci Technol* 2008;**68**:1718–26.
15. Han JC, Hu P, Zhang XH, Meng SH, Han WB. Oxidation resistant ZrB_2–SiC composites at 2200 °C. *Compos Sci Technol* 2008;**68**:799–806.

16. Monteverde F, Savino R. Stability of ultra-high-temperature ZrB_2–SiC ceramics under simulated atmospheric re-entry conditions. *J Eur Ceram Soc* 2007;**27**:4797–805.
17. Monteverde F, Savino R, De Stefano Fumo M, Di Maso A. Plasma wind tunnel testing of ultra-high temperature ZrB_2–SiC composites under hypersonic re-entry conditions. *J Eur Ceram Soc* 2010;**30**:2313–21.
18. Han JC, Hu P, Zhang XH, Meng SH. Characteristics and mechanisms of dynamic oxidation for ZrB_2–SiC based UHTC. *Key Eng Mater* 2008;**36**:8–372, 1722-6.
19. Di Maso A, Savino R, De Stefano M, Silvestroni L, Sciti D. Arc-jet testing on HfB_2–$TaSi_2$ models: effect of the geometry on the aerothermal behavior. *Open Aerosp Eng J* 2010;**3**:10–9.
20. Savino R, De Stefano Fumo M, Silvestroni L, Sciti D. Arc-jet testing on $HfB_2$and HfC-based ultra-high-temperature-ceramic materials. *J Eur Ceram Soc* 2008;**28**:1899–907.
21. Silvestroni L, Sciti D, Melandri C, Guicciardi S. Toughened ZrB_2-based ceramics with addition of SiC whiskers or chopped fibres. *J Eur Ceram Soc* 2010;**30**:2155–64.
22. Berger MH, Hochet N, Bunsell AR. Microstructure and thermo-mechanical stability of a low oxygen nicalon fibre. *J Microsc* 1995;**177**:230–41.
23. Savino R, De Stefano Fumo M, Paterna D, Serpico M. Aerothermodynamic study of UHTC-based thermal protection systems. *Aerosp Sci Technol* 2005;**9**:151–60.
24. Cubiciotti D. The melting point-composition diagram of zirconium–oxygen system. *J Am Ceram Soc* 1951;**75**:2032–5.
25. Vahlas C, Laanami F, Monhiux M. Thermodynamic approach to the oxidation of Hi-Nicalon fibers. *J Am Ceram Soc* 1999:2514–6.
26. Shimoo T, Morisada Y, Okamura K. Oxidation behavior of Si–C–O fibers (Nicalon) under oxygen partial pressures from 10^2 to 10^5 Pa at 1773 K. *J Am Ceram Soc* 2000;**83**:3049–56.
27. Silvestroni L, Sciti D. Oxidation of ZrB_2 ceramics containing SiC ad particles, whiskers or short fibers. *J Am Ceram Soc* 2011;**94**:2796–9.
28. Shimoo T, Okamura K, Morita T. Thermal stability of low-oxygen silicon carbide fibers (Hi-Nicalon) in carbon monoxide. *J Mater Sci* 2003;**38**:3089–96.
29. Parthasarathy TA, Rapp RA, Opeka M, Kerans RJ. A model for the oxidation of ZrB_2, HfB_2 and TiB_2. *Acta Mater* 2007;**55**:5999–6010.